

**CONTROLS ON SANDSTONE RESERVOIR QUALITY:
PERMIAN TO EARLY CRETACEOUS SEQUENCES,
BARROW SUB-BASIN, NORTH WEST SHELF, WESTERN
AUSTRALIA**

GHAZI MAHMMOD KRAISHAN

B.Sc. (Geology)

M.Sc. (Sedimentology)

Thesis submitted in fulfilment of the requirements

for the degree of

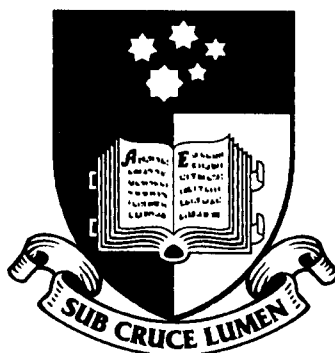
DOCTOR OF PHILOSOPHY

in

The National Centre for Petroleum Geology and Geophysics (NCPGG)

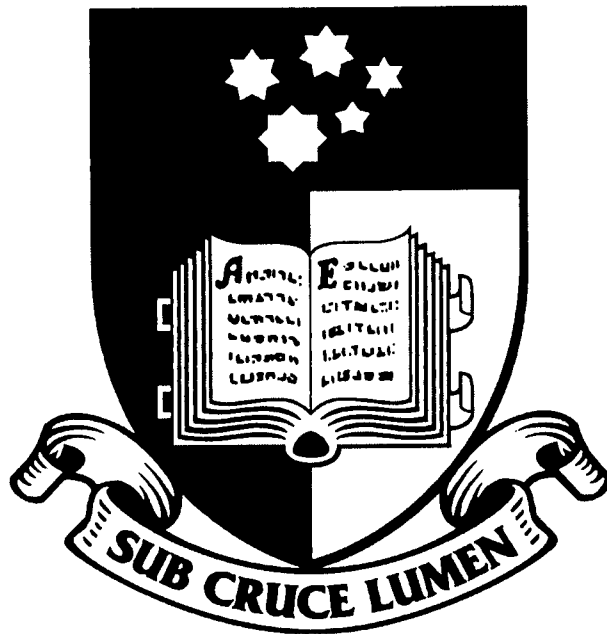
Of

The University of Adelaide



July 1997

STATEMENT OF AUTHENTICITY AND AVAILABILITY



This thesis contains no materials which has been accepted for the award of any other degree or diploma in any University. To the best of my knowledge and belief the thesis contains no materials previously published or written by another person, except where due reference is made in the text.

If accepted for the award of the degree and, if applicable, I consent to the thesis being made available for photocopying and loan.

Ghazi Kraishan

July 1997

Dedicated

To My Parents

And

To my Fiancée Deema

CONTROLS ON SANDSTONE RESERVOIR QUALITY: PERMIAN TO EARLY CRETACEOUS SEQUENCES, BARROW SUB-BASIN, NORTH WEST SHELF, WESTERN AUSTRALIA

Ghazi M. Kraishan

*National Centre for Petroleum Geology and Geophysics,
Thebarton Campus, The University of Adelaide,
GPO Box 498, Adelaide, South Australia, 5005.*

ABSTRACT

The Barrow Sub-basin, situated offshore on the North West Shelf of Australia, is one of the most prospective hydrocarbon among the provinces in the country with numerous commercial oil and gas accumulations. In spite of the number of papers written on the sub-basin, diagenetic effects on reservoir quality and the distribution of the porosity and permeability have received little attention.

The study examines the diagenetic history of the sandstones in the Barrow Sub-basin. The specific aim of this study is to investigate their diagenetic evolution and to determine both depositional and post-depositional factors that influenced the porosity, permeability and reservoir properties in the Barrow Sub-basin. Relative timing of these factors is determined and absolute timing is constrained by reference to factors such as exposure on unconformities, periods of rapid burial and compaction, heating events and major water migration episodes.

This integrated approach involves identification of all controls on the reservoir quality, including tectonic setting, burial history and clay minerals diagenesis, as well as the chemical evolution of the pore-water. The present reservoir properties described to ensure maximum hydrocarbon recovery and to predict reservoir quality in less explored areas. Techniques used include: interpretation of depositional environments; textural; chemical, isotopic and petrophysical analysis.

The sandstones of the Barrow Sub-basin were deposited in environments ranging from fluvio-deltaic to shelf to deep marine turbidites are generally extremely well sorted and display a unimodal grain-size distribution. These sediments have undergone a complex diagenetic history that can be related to pore-water evolution and to progressive burial history.

The precipitation of authigenic minerals has greatly reduced the reservoir quality of the Barrow Sub-basin sandstones. Fourteen authigenic minerals have been identified. Quartz, kaolinite and authigenic carbonate minerals are volumetrically significant, whilst glauconite, pyrite, feldspar, albite, other clay minerals and barite are present in minor to trace amounts. These authigenic minerals are distributed on a regional scale and cover a wide stratigraphic and depth range. Because these minerals are not all present in a single formation, a paragenetic sequence has been drafted which represents a composite sequence from different stratigraphic ages. This sequence is based on petrographic, isotopic and fluid

inclusion studies, all aided by the burial history curves. The geothermal gradients, the heat flow and the thermal history of sub-basin were taken into consideration during the interpretation of the sequence of diagenetic events.

Post-depositional precipitation of the authigenic minerals began early in the diagenetic history with the formation of glauconite fecal pellets. Shortly after deposition, framboidal pyrite started to precipitate during sulfate reduction followed by the precipitation of micritic siderites. An invasion of acidic meteoric waters occurred during a later uplift of the sub-basin, resulting in partial dissolution of feldspars and precipitation of an early feldspar overgrowths and kaolinite. Subsequent water modification resulted in local precipitation of poikilotopic calcite, which overlaps the previous authigenic minerals. In the middle stage of the diagenetic history and during the early maturation of the organic matter, early and second phases of the quartz overgrowths and siderite (sparry siderite) occurred. Later, ankerite cement was precipitated during deep burial from water expelled from the underlying shale and during smectite to illite conversion. The latest diagenetic mineral was probably cubic pyrite, which occurs in association with oil entrapment. The timing of barite precipitation and albitisation is uncertain.

Authigenic carbonate minerals reveal a complex evolution of the chemical and isotopic signatures of the pore-waters. The early authigenic carbonate minerals were precipitated from marine pore-water and have almost identical chemical and isotopic ratios. After the rifting of the sub-basin (Calloviaian mid-Jurassic), a slight uplift occurred and introduced meteoric water to the system along the eastern margin and resulted in precipitation of the middle stage carbonate phases. The later phases of carbonate occurred when the sandstone was buried enough to produce modified diagenetic water from the thick shale beds that underlying these sandstones. The strontium isotopic ratios are consistent with the model proposed by the carbon and oxygen isotopic ratios for the authigenic carbonates. The $^{87}\text{Sr}/^{86}\text{Sr}$ ratios of the early carbonate indicate an early occurrence from Cretaceous marine water. In contrast, the middle and late carbonate phases have higher Sr ratios, suggesting involvement of radiogenic Sr, which could be liberated from the dissolution of the silicate minerals or during the shale diagenesis.

Isotopic ratios of the cubic pyrite associated with oil, are extremely enriched with ^{34}S , indicating late precipitation during extensive sulfate reduction.

The reservoir quality is highly affected by depositional and post-depositional factors. Sandstones deposited in slope/basin marine environments contain abundant clay matrix, which may exceed 14 per cent of the whole-rock volume compared with about 7 per cent in the marine shelf environments. Transitional to non-marine environments have less than 3 per cent detrital clay matrix on average. In addition, it seems that the authigenic clays have developed mostly in those facies enriched in depositional matrix making the possibility of enhancement of reservoir quality complex.

Post-depositional factors, the precipitation of authigenic minerals and mechanical and chemical compaction, have worked together to reduce the primary intergranular porosity. In general, both processes have had nearly equal effect in destroying the original intergranular porosity. The precipitation of the authigenic minerals has reduced, on average, the primary intergranular porosity up to 15 per cent of the whole rock-volume. The mechanical and chemical compaction processes have further contributed to porosity loss. They show less

effect on porosity due to the rapid deposition of the sandstones and early precipitation of some authigenic minerals, which slightly inhibit the effects of compaction.

The development of secondary porosity has greatly enhanced the reservoir quality of the Barrow Sub-basin sandstones. More than one mechanism for the development of secondary porosity is apparent. The invasion of acidic meteoric water and the release of organic acids during organic-matter maturation have both played a significant part upon the enhancement of the reservoir quality. The first mechanism occurred during the several episodes of uplift which occurred during the development of the sub-basin. Organic acids released during the organic-matter maturation, migrated up-dip along the fault axes to develop secondary porosity of carbonate cemented zones. Secondary porosity developed by dissolution in carbonate-cements (especially calcite) has greatly enhanced the reservoir quality of the Barrow Sub-basin sandstones, especially around the basin margins, along the Rankin Trend and in the southern part of the sub-basin.

ACKNOWLEDGMENTS

I wish to thank the Australian Government represented by the Department of Employment, Education and Training (DEET) for the Overseas Postgraduate Research Scheme (OPRS) scholarship. The research project was sponsored and supported by the Australian Petroleum Co-operative Research Centre (APCRC), Mobil Exploration & Producing (Australia), Western Mining Corporation and Boral Energy Resources. The Adelaide University and the National Centre for petroleum Geology and Geophysics (NCPGG) are also acknowledged for the financial support and their living allowance scholarships.

I am extremely grateful to Dr. Nicholas Lemon, Senior Lecturer at the NCPGG, for his many valuable suggestions, his support and guidance and his friendship during my stay in Australia.

The author wishes to express his deep appreciation to Dr. Peter Tingate and Dr. Jay Matthews for their constructive and critical reading, discussions and their valuable suggestions

I appreciate the help provided by the technical staff of the Department of Geology and Geophysics. Particularly, Mr. J. Stanley for XRD analysis, Mr. W. Mussard for thin section preparation and help with fluid inclusion, and Mr. D. Bruce for strontium isotope supervision. Special thanks goes to Dr. K. Turnbull for his supervision with stable isotope processing. I also would like to thank the staff at Centre for Electron Microscopy and Microprobe Analysis (CEMMA), especially Mr. J. Terlet and Mr. H Rosser. I would like to thank the staff from the NATA laboratory at the Commonwealth Scientific & Industrial Research Organisation (CSIRO) Division of Soils (Adelaide South Australia), in particular Mr. J Dighton, for assistance in the formation water chemistry and isotope analyses.

Western Mining Corporation and Western Australia Petroleum Pty. Ltd (WAPET) kindly supplied the drill core samples, formation waters and much logistic support.

Special thanks to my second family at NCPGG Adelaide who made my life throughout this study joyful. The late Dr. William (Bill) J. Stuart, Prof. C. Griffiths, Prof. J. Applegate, Ms. Maureen Sutton and Mrs. B Wallis are greatly acknowledged. Also many thanks to my colleagues, the Jordanian fellow friend Khalid Al- Arouri and his family, S. Polomka, A. Kaiko, Tom (Mac) McGilvery, M. Rezaee and X. Sun for their assistance and moral support.

Finally, I would like to extend my gratitude to my family for their support and belief in me, as without their support none of this could have been achieved. To my other half, to my lovely fiancée Miss Deema Al- Sheikhly, for her encouragement, help, understanding and patience.

TABLE OF CONTENTS

ABSTRACT	i
ACKNOWLEDGMENTS	iv
TABLE OF CONTENTS	v
LIST OF FIGURES	ix
LIST OF TABLES	xvi
CHAPTER ONE INTRODUCTION	1
1.1 GENERAL INTRODUCTION	1
1.2 AIMS OF STUDY	2
1.3 PREVIOUS INVESTIGATIONS	3
1.4 METHODOLOGY	4
1.4.1 Sampling	4
1.4.2 Analytical Techniques	8
1.4.2.1 Petrography	8
1.4.2.2 X-ray mineralogy	8
1.4.2.3 Cathodoluminescence (CL) microscopy	9
1.4.2.4 Scanning electron microscope	9
1.4.2.5 Microprobe analysis	10
1.4.2.5 Carbon and oxygen isotopes	10
1.4.2.6 Strontium isotopes	11
1.4.2.7 Sulphur isotopes	11
1.4.2.8 Fluid inclusions	12
1.4.2.9 Water chemistry	13
1.4.2.10 Oxygen and deuterium isotopes	13
CHAPTER TWO REGIONAL GEOLOGIC SETTING	14
2.1 INTRODUCTION	14
2.2 TECTONIC SETTING	19
2.3 STRATIGRAPHY	21
2.4 BARROW SUB-BASIN PETROLEUM SYSTEM	24
2.4.1 Essential Elements of the Petroleum Systems	25
2.4.1.1 Petroleum Source Rocks	25
2.4.1.2 Reservoir Rocks	28
2.4.1.3 Seal Rocks	30
2.4.1.4 Overburden Rocks	30
2.4.2 Petroleum System Processes	32
2.4.2.1 Traps	32
2.4.2.2 Hydrocarbon Generation-Migration-Accumulation	33
2.5 EXPLORATION HISTORY	35
2.6 HYDROCARBONS	36
CHAPTER THREE LITHOFACIES ANALYSIS	38
3.1 INTRODUCTION	38
3.2 PERMIAN	40
3.2.1 Lithofacies Description	40
3.2.1.1 Facies 1: Interbedded siltstone and shale	40
3.2.1.2 Facies 2: Interbedded sandstone, siltstone and mudstone	41
3.2.1.3 Facies 3: Cross-stratified, horizontally laminated sandstones	42
3.3 TRIASSIC	43
3.3.1 Lithofacies Description and depositional environments	44
3.3.1.1 Unit "K"	44
3.3.1.2 Unit "J"	44
3.3.1.3 Unit "I"	44
3.3.1.4 Unit "H"	45
3.3.1.5 Unit "G"	45
3.3.1.6 Unit "F"	45

3.3.1.7 Unit "E"	45
3.3.1.8 Unit "D"	46
3.4 JURASSIC	46
3.4.1 Lithofacies of Dingo Claystone (Wulff, 1991, 1992)	47
3.4.1.1 Facies 1: Homogeneous, very fine to fine-grained sandstone	47
3.4.1.2 Facies 2: Very fine to medium-grained sandstone with abundant shale clasts	48
3.4.1.3 Facies 3: Very fine to coarse-grained, poorly sorted, argillaceous sandstone	48
3.4.1.4 Facies 4: Very fine to coarse-grained, bioturbated, argillaceous sandstone	48
3.4.1.5 Facies 5: Very fine to fine-grained, bioturbated argillaceous sandstone	49
3.4.1.6 Facies 6: Matrix supported, pebble to boulder-sized conglomerate	49
3.4.1.7 Facies 7: Medium to coarse-grained, well sorted, feldspathic sandstone	50
3.5 LOWER CRETACEOUS SEDIMENTS	50
3.5.1 Barrow Group (including Flag Sandstone)	52
3.5.1.1 Mounded Turbidite Lobe System	52
3.5.1.1.1 Facies 1: Massive sandstones, with horizontal to wavy lamination or ripple cross stratification	52
3.5.1.1.2 Facies 2: Interbedded to laminated, dark grey to black shale and cream sandstone beds	53
3.5.1.1.3 Facies 3: Massive to finely laminated shale, rare to common, thin sandstone laminae. ..	53
3.5.1.1.4 Facies 4: Rip-up clast bearing sandstone	54
3.5.1.1.5 Facies 5: Soft-sediment-deformed, interbedded shale and mud-rich sandstone	54
3.5.1.2 Slope Apron System	55
3.5.1.2.1 Facies 6: Mud-rich sandstone with intense convolute bedding	55
3.5.1.2.2 Facies 7: Stacked, upward-fining sandstones.	55
3.5.1.2.3 Facies 8: Massive, mud-rich sandstone.	55
3.5.1.3 Marine-reworked Strandplain System	56
3.5.1.3.1 Facies 9: Randomly interbedded, "clean" sandstones and mud-rich sandstones.	56
3.5.1.3.2 Facies 10: Stacked, thin-bedded sandstones to thin, interbedded sandstone and shale ...	57
3.5.1.3.3 Facies 11: Stacked, thin to thick bedded, large scale bioturbated sandstone.	57
3.5.1.3.4 Facies 12: Dune-scale, cross-stratified sandstone	58
3.5.1.3.5 Facies 13: Sandstone, thinning and fining upward, commonly grading to laminated shale capped by coal	59
3.5.1.3.6 Facies 14: Conglomerate.	60
3.5.2 Winning Group	62
3.5.2.1 Tunney Member	63
3.5.2.1 1 Facies 1: Bioturbated fine-grained sandstone	63
3.5.2.1 2 Facies 2: Upwards fining sandstone.	64
3.5.2.1 3 Facies 3: Upwards coarsening sandstone	64
3.6 SUMMARY	65
CHAPTER FOUR PETROGRAPHIC OBSERVATIONS AND DIAGENETIC HISTORY	74
4.1 INTRODUCTION	74
4.2 DETRITAL COMPOSITION OF BARROW SUB-BASIN SANDSTONES	74
4.2.1 Texture	74
4.2.2 Framework Grain Composition	78
4.2.2.1 Quartz	81
4.2.2.2 Feldspar	81
4.2.2.3 Rock fragments	89
4.2.2.4 Detrital clay matrix	89
4.2.2.5 Accessory minerals and organic matter	91
4.3 BARROW SUB-BASIN SANDSTONE COMPOSITION	91
4.3.1 Kennedy and Byro Groups	91
4.3.2 Mungaroo Formation	92
4.3.3 Barrow Group	92
4.3.4 Flag Sandstone	93
4.3.5 Tunney Member	93
4.4 XRD RESULTS AND INTERPRETATION	93
4.5 DIAGENETIC MODIFICATIONS	103
4.5.1 Compaction	103
4.6.2 Authigenic Minerals	107
4.6.2.1 Early Stage	107
4.6.2.1.1 Glauconite	108

4.6.2.1.2 Pyrite	108
4.6.2.1.3 Calcite(I).....	108
4.6.2.1.5 Siderite (I)	111
4.6.2.1.6 Feldspar Overgrowth	112
4.6.2.1.7 Calcite (II)	113
4.6.2.2 Intermediate Stage	114
4.6.2.2.1 Quartz	114
4.6.2.2.2 Kaolin	116
4.6.2.2.3 Dolomite and Ferroan dolomite	117
4.6.2.2.4 Siderite (II)	117
4.6.2.3 Late Stage Minerals	118
4.6.2.3.1 Ankerite	118
4.6.2.3.2 Clay Minerals	118
4.6.2.3.3 Kaolin Group	125
4.6.2.3.4 Pyrite (II)	125
4.6.3.4 Fracture filling minerals:	127
4.6.3.5 Trace authigenic minerals.....	127
4.7 DISTRIBUTION OF AUTHIGENIC MINERALS	127
4.8 HYDROCARBONS	138
4.9 DISCUSSION.....	140
4.9.1 POSSIBLE SOURCES OF SILICA	140
4.9.2 CLAY FORMATION	144
4.10 SUMMARY	148
CHAPTER FIVE CHEMICAL AND ISOTOPIC COMPOSITION OF AUTHIGENIC MINERALS AND RELATIONSHIP TO DIAGENESIS	178
5.1 INTRODUCTION.....	178
5.2 COMPOSITION OF AUTHIGENIC MINERALS	180
5.2.1 Authigenic carbonates.....	180
5.2.1.1 Calcite	180
5.2.1.2 Siderite	186
5.2.1.3 Dolomite and ferroan dolomite.....	191
5.2.1.4 Ankerite	194
5.2.2 Quartz overgrowth	196
5.2.3 Feldspar overgrowth	199
5.3 ISOTOPIC RATIOS OF AUTHIGENIC CARBONATE MINERALS	201
5.3.1 Oxygen-18.....	201
5.3.1.1 Calcite	201
5.3.1.2 Siderite	205
5.3.1.3 Dolomite.....	208
5.3.1.4 Ankerite.....	208
5.3.2 Carbon-13	209
5.3.3 Strontium 87/86 ratios.....	212
5.4 SOURCE OF CARBON.....	217
5.5 PALAEOTEMPERATURE OF AUTHIGENIC CARBONATE MINERAL FORMATION	226
5.6 SULPHUR ISOTOPIC RATIOS OF PYRITE NODULES	234
5.7 FLUID INCLUSIONS OF AUTHIGENIC MINERALS	236
5.7.1 Fluid Inclusions.....	236
5.7.2 Homogenisation Temperatures	237
5.8 COMPOSITION OF FORMATION WATERS	239
5.8.1 Cations	241
5.8.2 Anions	247
5.9 ISOTOPIC RATIOS OF THE FORMATION WATERS AND ASSOCIATED HYDROCARBONS	247
5.9.1 Formation Water	247
5.9.2 Hydrocarbons.....	249
5.10 DISCUSSION.....	250
5.10.1 Formation of Authigenic Carbonate Minerals	250
5.10.2 Diagenetic Sequence	252
5.10.3 Siderite as sea level indicator.....	255
5.10.5 Pore water evolution	257
5.11 IMPLICATIONS FOR PETROLEUM GEOLOGY	261

CHAPTER SIX RESERVOIR QUALITY	266
6.1 INTRODUCTION.....	266
6.2 DEVELOPMENT OF POROSITY	269
6.2.1 Primary Porosity	269
6.2.2 Microporosity.....	270
6.2.3 Secondary Porosity	271
6.3 THE INFLUENCE OF AUTHIGENIC MINERALS ON RESERVOIR QUALITY	272
6.4 DISCUSSION.....	274
6.4.1 Reservoir Quality	274
CHAPTER SEVEN CONCLUSIONS	280
REFERENCES	285
APPENDICES (ATTACHED ON 3 FLOPPY DISKS)	
APPENDIX I SYMBOL INDEX	
APPENDIX II CORE DESCRIPTION	

LIST OF FIGURES

Figure 1.1 Schematic diagram showing the progress of the work and the analytical procedures employed for this study. Numbers between the parentheses represent the number of the samples of each analysis	5
Figure 1.2 Location map of the Barrow Sub-basin, showing the wells studied	6
Figure 2.1 Tectonic map showing the main structural features of the Barrow Sub-basin and surrounding sub-basins, and the main hydrocarbon accumulations, (modified after McClure, et al.1988). See Figure 2.2 for cross section A-B	17
Figure 2.2 Cross section across the Barrow Sub-basin A-B, modified after Hocking (1990). See Figure 2.1 for location	18
Figure 2.3 Tectono-stratigraphic chart of the Permian to Cretaceous sedimentary sequences of the Barrow Sub-Basin, showing distribution of oil and gas accumulations and the main source rock intervals. W.SST. = Windalia Sand Member, A, B, C and D seismic facies in South Pepper area (Williams and Poynton, 1985), LEG. = Legendare Formation	22
Figure 2.4 Events chart of the Barrow Sub-basin petroleum systems. a) Dingo Claystone, b) Triassic Locker Shale, and c) Triassic Mungaroo Formation, indicating the essential elements and processes. (after Magoon and Dow, 1994)	26
Figure 2.5 Burial history and thermal maturation models for the Barrow Sub-basin source rocks. The oil and gas windows are shown relative to maximum present-day burial depth in a) Onslow-1 Peedumalh Shelf and c) Gorgon-1 Rankin Trend, and b) Fennel-1 has experienced hotter burial depth than present-day temperature. (from Kaiko, 1997, in preparation)	31
Figure 3.1 Core description for the channel lithofacies and the log response of the sandstone from Barrow Group (Flacourt Formation) in the Griffin-1. Note the DT response of the coal layer on top of the section. Core description from MCGilvery (1996)	61
Figure 4.1 Grain size distribution of the Barrow Sub-basin sandstones. V.C = very coarse, C = coarse, M = medium, F = fine and V.F = very fine	79
Figure 4.2 QFR ternary diagram showing the present-day framework grain compositions of the Barrow Sub-basin sandstones: a) Permian sandstones are classified as quartzarenite, subarkose and sublitharenite (n = 10 samples), b) Triassic Mungaroo Formation sandstones are classified as quartzarenite, subarkose, lithic arkose and sublitharenite (n = 65 samples, (Jong, 1996)), c) Malouet Formation sandstones are quartzarenite, subarkose and sublitharenite (n = 15 samples), d) Flacourt Formation sandstones are classified as quartzarenite, subarkose and sublitharenite (n = 35 samples), e) Flag Sandstone sandstones are classified as quartzarenite and subarkose (n = 15) and f) Tunney Member sandstones are classified as subarkose (n = 5 samples). (after Folk, 1974)	80

Figure 4.3 Distribution of the average present day and original feldspar content in different depositional facies. Depositional facies scheme is adapted from McGilvery (1996). For depositional facies details and abbreviation used see Chapter 3	90
Figure 4.4 Distribution of the average depositional clay matrix content in different depositional facies. Depositional facies scheme is adapted from McGilvery (1996). For depositional facies details and abbreviation used see Chapter 3	90
Figure 4.5 XRD patterns for some sandstones from the Barrow Sub-basin. a) Flacourt Formation, Roller-1, 910.7 m, showing calcite cement, b) Kennedy Group, Onslow-1, 2166.5 m, showing ankerite cement, c) Flacourt Formation, West Pepper-1, 1394.4m, showing the double siderite peak which indicates a magnesium-rich siderite. Q = Quartz, F = Feldspar, K = Kaolinite, M = Mica, Ca = Calcite, A = Ankerite, S = Siderite and P = Pyrite	101
Figure 4.6 Abundance of authigenic carbonate minerals in the Barrow Sub-Basin sandstones. Number of samples based on petrographic observations (point count data). Mungaroo Formation and Dingo Claystone data are not presented in this figure	102
Figure 4.7 Abundance of the main authigenic minerals in the Barrow Sub-Basin sandstones. Number of samples based on XRD and petrographic observations. Mungaroo Formation and Dingo Claystone data are not presented in this figure	102
Figure 4.8 Intergranular volume vs. total cement diagram for the Barrow Sub-basin sandstones used to evaluate the relative importance of compaction and cementation processes to porosity reduction. (after Houseknecht, 1987; 1989 and modified after Ehrenberg, 1989; 1990). * represents the average in each formation. a) * represents the average of Byro Group sandstones (◆ 4 samples from 2 wells), and * represents the average of Kennedy Group sandstones (● 4 samples from 2 wells), b) Mungaroo Formation 64 samples from 13 wells (from Jong, 1996), c) Malouet Formation 25 samples from 5 wells, d) Flacourt Formation 66 samples from 13 wells, e) Flacourt Formation in Griffin-1 and f) Flag Sandstone 12 samples from 4 wells	104
Figure 4.9 X-ray diffractogram traces of the < 2 µm oriented fraction of the background sandstone of Birdrong Formation from Griffin-2, 2660.30 m. The clay fraction is dominated by chlorite and low expandable illite/smectite mixed-layer. (d-spacings in Angstroms. Co K α radiation)	121
Figure 4.10 X-ray diffractogram traces of the < 2 µm oriented fraction from siltstone in the Toolonga Calcilutite from Georgete-1, 300.0m. The clay fraction is dominated by highly expandable and randomly interstratified illite/smectite and vermiculite. (d-spacings in Angstroms. Co K α radiation)	122

Figure 4.11 Diffractograms (Co K α radiation) of < 2 μm fractions from different depths, formations and wells to show the degree of ordering in illite/smectite mixed-layer composition and its variation with burial depth. a) randomly interstratified (R0) with around 50% illite, b) randomly interstratified (R0) with around 60% illite, c) regular interstratified (R1) with about more than 70-80% illite, d) regular interstratified with (R1) with about 80% illite, and e) ordered (R3) illite/smectite mixed-layer with about more than 80% illite	124
Figure 4.12 X-ray diffractogram traces of the < 2 μm oriented fraction from the Muderong Shale in Pasco-1, 1160.4m. The clay fraction is dominated by mixed layer glauconite and smectite. (d-spacings in Angstroms. Co K α radiation)	126
Figure 4.13 EDS spectrum for euhedral albite crystal on the surface of detrital grain K-feldspar grain showing no Ca, Malouet Formation, Barrow-25, 1992.5m	128
Figure 4.14 EDS spectrum for detrital K-feldspar grain showing no Ca or Na, from Malouet Formation, Barrow-25, 1992.5 m	128
Figure 4.15 Cement distribution within the Permian Byro and Kennedy Groups in the Barrow Sub-basin, showing the wells studied. Quartz overgrowths, kaolinite and siderite are ubiquitous	130
Figure 4.16 Cement distribution of Mungaroo Formation sandstones of the Barrow Sub-basin, showing the wells studied. Modified after Kraishan and Jong (1995) and Jong (1996). Quartz overgrowths, kaolinite and siderite are ubiquitous	131
Figure 4.17 Cement distribution within the Barrow Group sandstones in the Barrow Sub-basin, showing the wells studied. Quartz overgrowths, kaolinite and siderite are ubiquitous	132
Figure 4.18 Common authigenic minerals in Barrow Sub-basin and their distribution vs. depth. There is no systematic correlation between any of the authigenic minerals and depth. a) Note the relation between authigenic calcite and depth indicating an early diagenetic origin of the calcite cement. The relatively rare calcite cement below 2500 depth can be attributed to either dissolution of this mineral during burial diagenesis or non deposition. b) Dolomite includes Fe-dolomite and ankerite, the precipitation of dolomite minerals has occurred middle to late in the diagenetic history. c) Siderite is present in the shallower depths indicating an early to middle diagenetic occurrence. d) Quartz overgrowth relatively increases with depth. e) Kaolinite began early in the diagenetic environment and continued throughout burial. f) Pyrite has precipitated both as early and late, with the main phase during oil entrapment	134
Figure 4.19 Schematic diagram showing distribution of the main authigenic minerals with various depositional facies. For depositional facies details see Chapter 3 and Table 3.2, the facies scheme is modified from McGilvery (1996)	135
Figure 4.20 Average authigenic mineral content for different formations and stratigraphic ages	136

Figure 5.1 Inverse relationship between Ca and Mg in a microprobe traverse across early cavity-filling calcite. L82G, Gearle Siltstone, 347.0m	184
Figure 5.2 Fe and Mn composition of early calcite cements from Gearle Siltstone L82G, 347.0m in the Barrow Sub-basin plotted in the CL response diagram of Mason (1987). (Modified by Machel et al. 1991)	184
Figure 5.3 Composition of authigenic carbonate minerals a) calcite cements based on 179 analyses, b) dolomite, ferroan dolomite and ankerite based on 317 analyses and c) siderite cements based on 274 analyses	185
Figure 5.4 Inverse relationship between Fe and Mg in the micritic mixed marine/meteoritic siderite of the Malouet Formation, Barrow Group	190
Figure 5.5 Variable chemical composition of a single siderite crystal. Up to 9 different zonations were detected using BSE image analyses. Pasco-1, Windalia Sand Member, 975.1m	190
Figure 5.6 A microprobe-step traverse across a single saddle dolomite crystal shows multiple sharp contrasts between Fe and Mg between Fe rich and iron-poor zones. A 2- μ m size beam spot was used for these analyses. Yammaderry-1, Flacourt Formation, 1122.0m	192
Figure 5.7 Inverse relationship between trace elements in a single crystal of saddle dolomite. Yammaderry-1, Flacourt Formation, 1122.0m	192
Figure 5.8 Fe and Mn composition of dolomite sample from Yammaderry-1, Flacourt Formation, 1122.0m, plotted on the CL response diagram of Mason (1987). (Modified by Machel et al. 1991)	193
Figure 5.9 Inverse relationship between Mg and Fe in a single ankerite crystal. Flinders Shoal-1, Mungaroo Formation, 2009.5m	195
Figure 5.10 Variable composition across a single ankerite crystal. Note the sharp contrast indicating sudden change in the chemical composition of the pore water from which ankerite precipitated. Flinders Shoal-1, Mungaroo Formation, 2009.5m	195
Figure 5.11 A microprobe-step traverse across single ankerite crystal shows very sharp to gradational contacts between different zones indicating that pore water was fluctuating gradually during the precipitation of ankerite cements. Distance in 2- μ m. Flinders Shoal-1, Mungaroo Formation, 2009.5m	202
Figure 5.12 Isotopic composition ratios ($\delta^{13}\text{C}$ vs. $\delta^{18}\text{O}$) of authigenic carbonates in the Barrow Sub-basin sandstone sequences. Total number of the samples = 42. For sample locality refer to Table 5.4	202
Figure 5.13 Variation $\delta^{18}\text{O}$ and $\delta^{13}\text{C}$ values with depth in calcite cement. Early cavity-filling calcite, poikilotopic and late calcite cements	206

Figure 5.14 Relation between $\delta^{18}\text{O}$ and $\delta^{13}\text{C}$ values in calcite cement. Early cavity-filling calcite, poikilotopic and late calcite cements	206
Figure 5.15 Variation of $\delta^{18}\text{O}$ and $\delta^{13}\text{C}$ values of siderite cement with depth	207
Figure 5.16 Oxygen versus carbon isotopic ratios of the siderite cement	207
Figure 5.17 Variation of $\delta^{18}\text{O}$ and $\delta^{13}\text{C}$ values with depth in dolomite cements	208
Figure 5.18 Isotopic composition ($\delta^{13}\text{C}$ vs. $\delta^{18}\text{O}$) of authigenic ankerite reported in the literature compared to that of Barrow Sub-Basin ankerites. \circ Permian (Kennedy Group) ankerites, \blacktriangledown Triassic (Mungaroo Formation) ankerites	210
Figure 5.19 Distribution of δ carbon-13 relative to PDP in variable carbonate authigenic minerals of Barrow Sub-basin sandstones. a) calcite cement, b) siderite cements, c) dolomite and ferroan dolomite cements, and d) ankerite	211
Figure 5.20 Distribution of δ carbon-13 relative to PDP in variable carbonate authigenic minerals in all samples of Barrow Sub-basin sandstones	211
Figure 5.21 Distribution of strontium isotope ratios of variable authigenic carbonate minerals in Barrow Sub-basin sandstones	216
Figure 5.22 Oxygen versus strontium isotopes of the carbonate authigenic minerals in Barrow Sub-basin sandstones	216
Figure 5.23 Distribution of siderite cement in different depositional facies of the Barrow Sub-basin sandstones. Depositional scheme after McGilvery (1996) (see Chapter Three for more details)	222
Figure 5.24 Diagram illustrating effect of varying sedimentation rate and rate of organic-carbon oxidation on $\delta^{13}\text{C}$ values with depth. (after Mozley and Burns, 1993)	222
Figure 5.25 Formation water $\delta^{18}\text{O}$ values versus temperature for authigenic carbonate minerals a) early calcite concretion (upper curve) and vein-filling calcite, b) early meteoric siderite (higher curve), mixed marine-meteoric early siderite (middle curve) and early marine siderite (lower curve), c) poikilotopic calcite from Birdrong Formation (lower curve) and from Flacourt Formation (higher curve), d) Siderite II, e) dolomite and ferroan dolomite and f) ankerite Permian ankerite (lower curve) Triassic ankerite from Eastern Shelf (middle curve) and Triassic of Rankin Trend (upper curve). Calculation where performed using the following mineral-water fractionation equations: a) and c) $1000\ln\alpha(\text{calcite-water}) = 2.78 \times 10^6 T^{-2} - 2.89$ (Friedman and O'Neil, 1977); b) and d) $1000\ln\alpha(\text{siderite-water}) = 3.13 \times 10^6 T^{-2} - 3.5$ (Carothers et al. 1988); e) $1000\ln\alpha(\text{dolomite-water}) = 3.2 \times 10^6 T^{-2} - 1.5$ (Land, 1983); f) $1000\ln\alpha(\text{ankerite-water}) = 2.78 \times 10^6 T^{-2} + 0.11$ (Fisher and Land, 1986). T = Temperature in Kelvin	228

Figure 5.26 Measured homogenisation temperatures for both quartz overgrowths and ankerite cement. Homogenisation temperatures for three quartz overgrowth phases are shown, with present temperature for each sample (arrows). Samples from a to d are for quartz overgrowth. a) ONS-16 2491.7m, present day temperature ~ 110°C, b) GR1-2 2714.7m, present temperature ~ 112°C, c) GR1-4 2707.2m, d) BO1-13, 3604.0m, present temperature ~140°C and, e) ONS-16, 2491.7m, ankerite present-day temperature ~ 110°C	238
Figure 5.27 Chemical composition of South Pepper formation water, Barrow Sub-basin	242
Figure 5.28 Composition of South Pepper formation waters (white circles) with relative to the seawater (solid circle)	243
Figure 5.29 Distribution of different cations and anions as a function of salinity (TDS) of South Pepper formation waters	244
Figure 5.30 Comparison of some cation concentrations of South Pepper formation water with an evaporation of seawater; a) sodium, b) potassium, c) calcium, d) magnesium and e) strontium (normal evaporite curves after Collins, 1975)	245-246
Figure 5.31 Isotopic composition of South Pepper formation water. Note that all samples lie to the right of the Meteoric water line indicating a probable mixture of meteoric and older formation waters	248
Figure 5.32 Schematic plot of δD and ^{18}O ‰ SMOW values indicating the effects of various mixing and fractionating processes on the isotopic composition of water (after Hitchon et al. 1971)	248
Figure 5.33 Generalised sequence of the diagenetic events of the sandstone reservoirs of the Barrow Sub-Basin. Timing is based on petrographic relationships and the temperature interpretation is based on isotopic studies. The shaded area represents the possible timing of oil entrapment and emplacement	254
Figure 5.34 System tracts as represented by increments on a hypothetical relative sea level curve. (after I. Dyson NCPGG, University of Adelaide, unpublished data)	258
Figure 5.35 Pore-water evolution path for the Barrow Sub-basin waters as inferred from stable isotope and fluid inclusion data	260
Figure 6.1 Mean grain size against depositional environments of Barrow Group. The grain size of SC, G2 and G3 facies was not estimated. The grain size, in general, decreases from channel or mound facies (MC) to small-scale slump facies (MF) and increases from amalgamated turbidite facies (AT) to the tidal-channel facies (TC). Depositional environments are elaborated in Table 6.1	267
Figure 6.2 Distribution of primary and secondary porosities in different depositional facies of Barrow Group sandstones. Depositional environments are elaborated in Table 6.1	269

Figure 6.3 Both intergranular and secondary porosity, as indicated from thin section point counts, decrease with depth in the samples studied of Barrow Group sandstones. Intergranular porosity is highly variable indicating factors other than compaction from depth of burial are active. Secondary porosity at shallow depths is suggestive of a meteoric influence in dissolution270

Figure 6.4 Plot of primary intergranular porosity versus total cement in the Flacourt Formation of Barrow Group. Correlation coefficient = -0.60274

Figure 6.5 Distribution of reservoir quality in the different depositional environments of the Barrow Group sandstones. Details of lithofacies are shown in Table 6.1275

Figure 6.6 Plot of the relation between depositional matrix and intergranular primary porosity in different depositional environments of Barrow Group sandstones276

Figure 6.7 Distribution of total porosity and permeability (selected core data) versus depth of Barrow Group sandstones. There is a general trend of decreasing in porosity and permeability with depth but with considerable variability277

LIST OF TABLES

TABLE 1.1 Groups and formations sampled for the regional diagenetic study in the Barrow Sub-basin	7
TABLE 2.1 Oil and gas fields in the Barrow Sub-basin area, Western Australia	15-16
TABLE 3.1 Well studied and logged from Barrow Sub-basin for lithofacies analysis	38
TABLE 3.2 Lithofacies scheme and depositional facies used for core description. Lithofacies scheme modified from Miall (1978) and the depositional facies from McGilvery (1996)	39
TABLE 4.1 Grain size data from Barrow Sub-basin sandstones	75-77
TABLE 4.2 Grain size variations of Barrow Sub-basin sandstones with different depositional environments. Facies scheme modified after McGilvery (1996)	79
TABLE 4.3 Modal composition of the Barrow Sub-basin sandstone reservoirs. Data in this table represent different stratigraphic ages from Early Permian to Early Cretaceous, based on petrographic observations. Analyses were derived by counting between 300-1000 points per thin section	82-88
TABLE 4.4 Bulk x-ray diffraction results of samples from Barrow Sub-basin Sandstones	94-100
TABLE 4.5 The effect of compactional processes on the primary intergranular porosity of the Barrow Sub-basin sandstones	105
TABLE 4.6 Mineralogical composition of < 2 μ m Clay fractions of the Barrow Sub-basin sediments	120
TABLE 5.1 Chemical composition of authigenic carbonate minerals, Barrow Sub-basin Sandstones	181-182
TABLE 5.2 Chemical analyses of the quartz overgrowths and detrital quartz grains of Barrow Sub-basin sandstones. (Values in ppm)	187-188
TABLE 5.3 Electron microprobe analyses of authigenic feldspar overgrowth and detrital feldspar of the Barrow Sub-basin sandstones	200
TABLE 5.4 Stable isotope composition ($\delta^{13}\text{C}_{\text{PDB}}$ & $\delta^{18}\text{O}_{\text{SMOW}}$) of the authigenic carbonate minerals of the Barrow Sub-basin sandstones	203-204
TABLE 5.5 $^{87}\text{Sr}/^{86}\text{Sr}$ isotope composition of some authigenic carbonate minerals of the Barrow Sub-basin sandstones	215
TABLE 5.6 Sulfur isotope results of pyrite nodules and cement in the Barrow Sub-basin Sandstones	235

TABLE 5.7 Well data and chemical and isotopic analysis of South Pepper Formation waters in Barrow Sub-basin	240
TABLE 5.8 Concentration ratios of South Pepper Field formation water	242
TABLE 6.1 Summary of the depositional characteristics, reservoir quality, grain size, distribution and degree of cementation in each Barrow Group facies	268
TABLE 6.2 The effect of compactional and cementation processes on primary intergranular porosity of Barrow Group sandstones	273
TABLE 6.3 Summary of the petrographic point-count data for the Barrow Group sandstones. Values are in per cent. Grain size in mm and sorting in ϕ degrees of Beard and Weyl (1973)	273